

## Article

# Glassy Carbon Electrode Modified with N-Doped Reduced Graphene Oxide Sheets as an Effective Electrochemical Sensor for Amaranth Detection

Hediyeh Moradpour <sup>1</sup>, Hadi Beitollahi <sup>2,\*</sup>, Fariba Garkani Nejad <sup>1</sup> and Antonio Di Bartolomeo <sup>3,\*</sup> 

<sup>1</sup> Department of Chemistry, Graduate University of Advanced Technology, Kerman 7631885356, Iran; hediyehmoradpour2020@gmail.com (H.M.); f.garkani95@gmail.com (F.G.N.)

<sup>2</sup> Environment Department, Institute of Science and High Technology and Environmental Sciences, Graduate University of Advanced Technology, Kerman 7631885356, Iran

<sup>3</sup> Department of Physics "E.R. Caianaiello", University of Salerno, 84084 Fisciano, Salerno, Italy

\* Correspondence: h.beitollahi@kgut.ac.ir (H.B.); adibartolomeo@unisa.it (A.D.B.)

**Abstract:** Amaranth is one of the synthetic azo colorants used to improve the appearance and to increase the appeal of some foods and soft drinks. The excessive consumption of amaranth can be associated with health side effects, emphasizing the need to monitor this food dye. Accordingly, the present study aimed to introduce an electrochemical sensor of glassy carbon electrode (GCE) modified with N-doped reduced graphene oxide (N-rGO), N-rGO/GCE, to detect the amaranth sensitively and rapidly. Several electrochemical techniques such as differential pulse voltammetry (DPV), linear sweep voltammetry (LSV), chronoamperometry (CHA), and cyclic voltammetry (CV) are exploited for the evaluation of the efficiency of the developed electrode for the detection of amaranth. We found that N-rGO/GCE enhanced amaranth oxidation, thus significantly elevating the current signal. Amaranth showed that calibration curves ranged from 0.1 to 600.0  $\mu\text{M}$ , and the limit of detection (LOD) ( $S/N = 3$ ) was 0.03  $\mu\text{M}$ . Finally, the developed sensor was effectively applied for real samples (tap water, apple juice, and orange juice) with acceptable recovery values from 96.0 to 104.3%.

**Keywords:** reduced graphene oxide; electrochemical sensor; amaranth; N-doped reduced graphene oxide; glassy carbon electrode



**Citation:** Moradpour, H.; Beitollahi, H.; Nejad, F.G.; Di Bartolomeo, A. Glassy Carbon Electrode Modified with N-Doped Reduced Graphene Oxide Sheets as an Effective Electrochemical Sensor for Amaranth Detection. *Materials* **2022**, *15*, 3011. <https://doi.org/10.3390/ma15093011>

Academic Editor: Rosalinda Inguanta

Received: 19 March 2022

Accepted: 18 April 2022

Published: 21 April 2022

**Publisher's Note:** MDPI stays neutral with regard to jurisdictional claims in published maps and institutional affiliations.



**Copyright:** © 2022 by the authors. Licensee MDPI, Basel, Switzerland. This article is an open access article distributed under the terms and conditions of the Creative Commons Attribution (CC BY) license (<https://creativecommons.org/licenses/by/4.0/>).

## 1. Introduction

3-hydroxy-4-[(4-sulfo-1-naphthalenyl)azo]-2,7-naphthalenedisulfonic acid trisodium salt, amaranth, belongs to synthetic pyrazolone colorants [1]. Some characteristics such as persistent stability and low cost made it an appropriate candidate to form red color in several sweets, drinks, and syrups [2,3]. Despite the presence of the azo functional group and structure of aromaticity, the excessive consumption of amaranth can be associated with human health side effects, including anxiety, allergies, dizziness, and even cancer. Accordingly, the United States have recognized the ban on the use of amaranth in food, and China has allowed the use of this colorant with a maximum acceptable range of 0.05 g/kg in soft drinks [4,5]. In fact, it should be concluded that achieving a fast and sensitive analytical approach is a basic need in the detection of amaranth in different food products.

Amaranth has been detected by different techniques, including thin layer chromatography (TLC) [6], high-performance liquid chromatography (HPLC) [7], liquid chromatography-mass spectrometry (HPLC-MS) [8], spectrophotometry [9,10], capillary electrophoresis (CE) [11], and electrochemical methods [12–14]. Some specific problems of these methods including the time-consuming extraction processes and expensive instrumentation, complex analysis processes, and the presence of interferences have limited their applications. Electrochemical methods are gaining popularity due to their special properties, including simplicity, rapid response, simple equipment, ease of use, and cost-effectiveness compared

with certain analytical techniques [15–21]. In addition, the reason for the increasing attention toward the modification of such electrodes can be attributed to the poor function of common electrodes in the detection of analytes [22–31]. The findings documented that the electron transfer rate can be increased and the overpotential can be significantly reduced through electrode surface modification.

Recently, nanomaterials have been widely used in various fields due to their exceptional properties [32–39]. The use of nanomaterials improves electrocatalytic properties and increases electrochemically active surface areas [40–48]. Graphene is a 2D nanostructure containing one or more sheets composed of carbon atoms. Therefore, it is one of the appropriate candidates to fabricate sensitive and selective sensors because of special features, including great electrical conductivity, high mechanical and thermal properties, and high specific surface area [49]. According to exceptional electronic potentials, graphene-based electrodes are able to enhance the electron transfer rate, suggesting a novel approach to develop electrochemical biosensors and sensors [50–52].

More recently, semiconductor-like properties can be achieved by chemically doped graphene, and charge conductivity and chemical reactivity can be enhanced by N-/P-doped graphene [53]. Nitrogen is one of the dopants with unique properties such as atomic radius close to that of carbon [54]. The electronic band structure can be controlled by doped N atoms. Moreover, mechanical strength, greater chemical stability, and special electronic properties have been reported for the N-doped graphene sheets [55] as a new material with various electrochemical purposes, such as the fabrication of sensors [56–59].

Thus, in this work, we developed a new electrochemical sensor to detect amaranth, in which a GCE was modified with N-rGO. The proposed method has advantages such as high linear dynamic range, high sensitivity, and a low limit of detection. Furthermore, this sensor successfully detected amaranth in real samples.

## 2. Experimental Section

### 2.1. Instruments and Chemicals

All electrochemical determinations were recorded by means of an Autolab potentiostat/galvanostat (PGSTAT-302N, Eco Chemie, Utrecht, The Netherlands). We exploited a single component three-electrode cell with a platinum auxiliary electrode and an Ag/AgCl (3 M KCl) reference electrode to perform the measurements. We used N-rGO/GCE as the working electrode while a Metrohm 827 pH meter (Metrohm AG, Herisau, Switzerland) was exploited to control the pH of the solutions. Analytical grade chemicals such as amaranth and other reagents were from Sigma-Aldrich and used as received.

### 2.2. Synthesis of N-rGO Sheets

The N-rGO sheets were prepared by a simple hydrothermal method. Firstly, exfoliated GO (100 mg) was dispersed by ultrasonication in deionized water (100 mL), and the pH of the above solution was adjusted to pH = 10 by dropwise adding ammonia solution ( $\text{NH}_3 \cdot \text{H}_2\text{O}$  (wt. 30%)). Next, urea (6.0 gr) was added and ultrasonicated for three hours. Then, the prepared solution was kept in an autoclave reactor at 180 °C for 12 h. After the autoclave reached ambient temperatures (25 °C), the samples were separated by centrifuge, washed several times by using deionized water, and its pH was adjusted to neutral. At last, the products (N-rGO sheets) were freeze-dried.

### 2.3. Preparing the Electrode

The synthesized N-rGO sheets were used for the modification of a GCE to prepare N-rGO/GCE. For this purpose, N-rGO suspension (1 mg/mL) in deionized water was prepared, and 4  $\mu\text{L}$  of the N-rGO suspension was drop casted onto the GCE surface and allowed to dry completely in ambient conditions.

### 3. Result and Discussion

#### 3.1. Characterization of N-rGO Sheets

A comparison of the FT-IR spectrum of GO and N-rGO is given in Figure 1. In the characteristic spectrum of GO, various functional groups in the structure include the vibration modes of O-H ( $3428\text{ cm}^{-1}$ ), C=O ( $1720\text{ cm}^{-1}$ ), C=C ( $1577\text{ cm}^{-1}$ ), phenolic C-O ( $1381\text{ cm}^{-1}$ ), and epoxy C-O-C ( $1038\text{ cm}^{-1}$ ). These index peaks indicate that there are several oxygen-containing functional groups (hydroxyl, epoxy, and carboxyl) on the surface of GO. Moreover, for N-rGO, the absence of absorption peaks of oxygen groups indicated that GO has been effectively reduced during the hydrothermal treatment. In addition, there are two peaks at  $1562\text{ cm}^{-1}$  and  $1184\text{ cm}^{-1}$ , which can be attributed to C=N (sometimes C=C and C=N bonds can stretch at the same wavelength) and C-N. This result confirmed that Gr was successfully N-doped. The FT-IR spectrum of the as-prepared sample was consistent with previous reports [60–62].

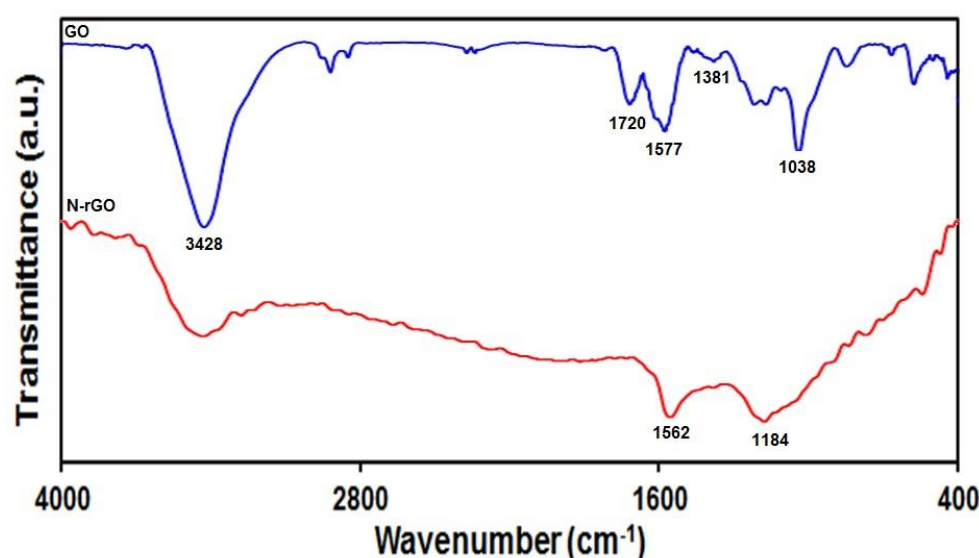


Figure 1. FT-IR spectrum of GO and N-rGO.

GO and N-rGO were characterized by XRD (Figure 2). The XRD pattern of GO depicts a sharp absorption peak at  $2\theta = 11.5$ , with an inter-planer space of  $7.69\text{ \AA}$ . GO possesses a larger inter-planer space compared to graphite due to the presence of  $\text{H}_2\text{O}$  molecules and various oxygen groups on its surface. In comparison, the XRD pattern of N-rGO confirmed the high reduction degree, as depicted in Figure 2. After hydrothermal process and in addition to the nitrogen-doping process, the peak at  $2\theta = 11.5$  disappeared, pointing to the successful reduction of GO. However, a broad absorption peak at around  $24.7^\circ$  appeared in N-rGO pattern [63], which can be attributed to an inter-planer distance of  $3.602\text{ \AA}$ , proving the existence of  $\pi$ - $\pi$  stacking between Gr layers [64].

The FE-SEM image of N-rGO, presented in (Figure 3) showed that N-rGO still maintain the 2D ultrathin flexible structure of the pristine Gr. Moreover, rGO sheets showed a wave structure that was similar to a thin, wrinkled paper. These results demonstrated the efficient N-doped process for the Gr. The FE-SEM image of as-prepared sample was consistent with previous reports [63,65,66].

#### 3.2. Electrochemical Behaviour of Amaranth at the Various Surface of Electrodes

The obtained results indicate that amaranth electro-oxidation occurred through electron and proton exchange. Furthermore, the optimization of the pH value in detecting the analyte was necessary. We used the DPV technique to explore the electrochemical response of amaranth on the N-rGO/GCE surface in phosphate buffer solution (PBS, 0.1 M) for pH ranging from 2 to 9. What is noteworthy is that the amaranth electro-oxidation on the

N-rGO/GCE surface, in neutral conditions, was higher than in alkaline or acidic medium. Accordingly, the value of 7.0 was chosen as the optimal pH for amaranth electro-oxidation on the N-rGO/GCE's surface.

The electrochemical performance of N-rGO/GCE in comparison with bare GCE was studied by the CV technique at exposure to 100.0  $\mu\text{M}$  of amaranth at 50 mV/s in PBS (0.1 M). The CVs of all as-fabricated electrodes in this study can be observed in Figure 5. The N-rGO/GCE voltammetric behavior (curve b) exhibited the relatively strongest and most characteristic anodic peak at 560 mV, sequentially. The bare GCE voltammetric behaviour (curve b) exhibited a relatively weak oxidation peak with less intensity at 860 mV, sequentially. Consequently, N-rGO/GCE has obviously better electrocatalytic behaviour than the bare GCE towards the amaranth with the relatively strong current response.

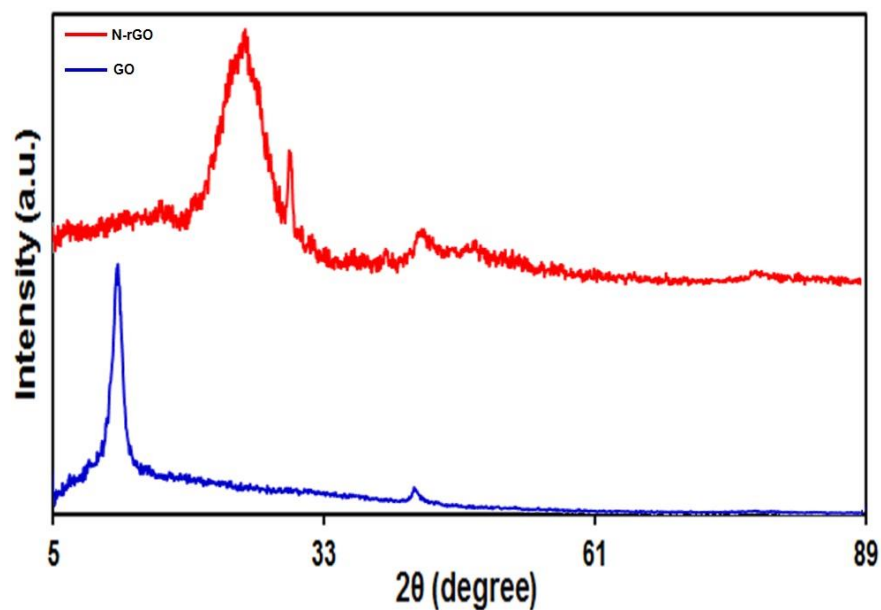


Figure 2. XRD pattern of GO and N-rGO.

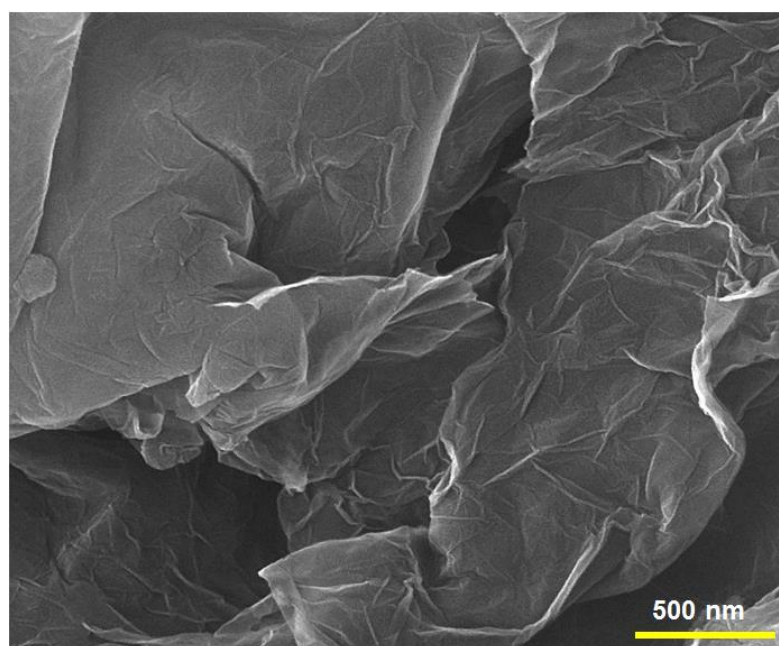


Figure 3. The FE-SEM image of N-rGO sheets.

We exploited energy dispersive X-ray spectroscopy (EDS) techniques for the analysis of elemental compositions (Figure 4). The EDS analysis showed that N-rGO sheets contain C, N, and O elements. This result demonstrated that the efficient N-doped process for rGO.

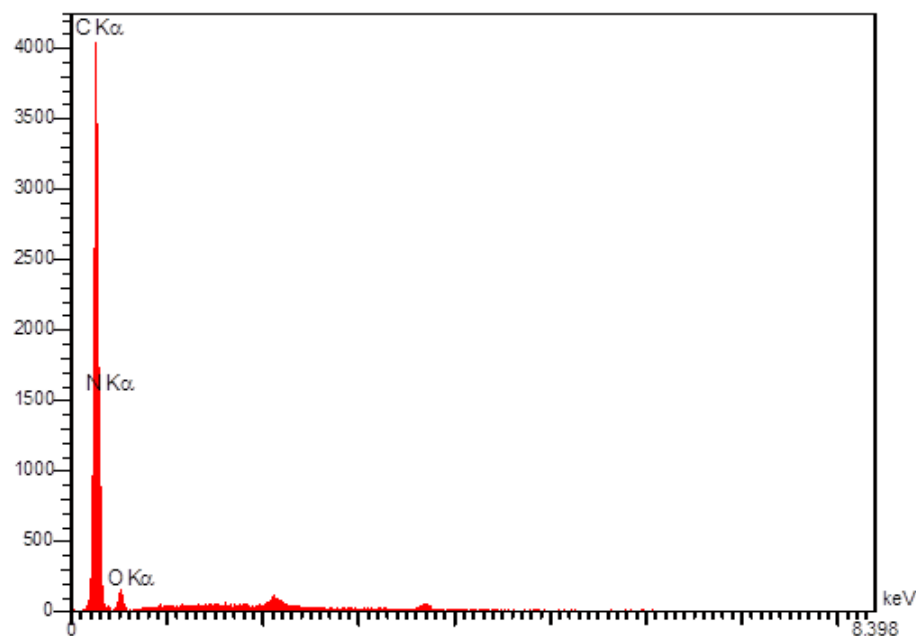


Figure 4. The EDS analysis of N-rGO.

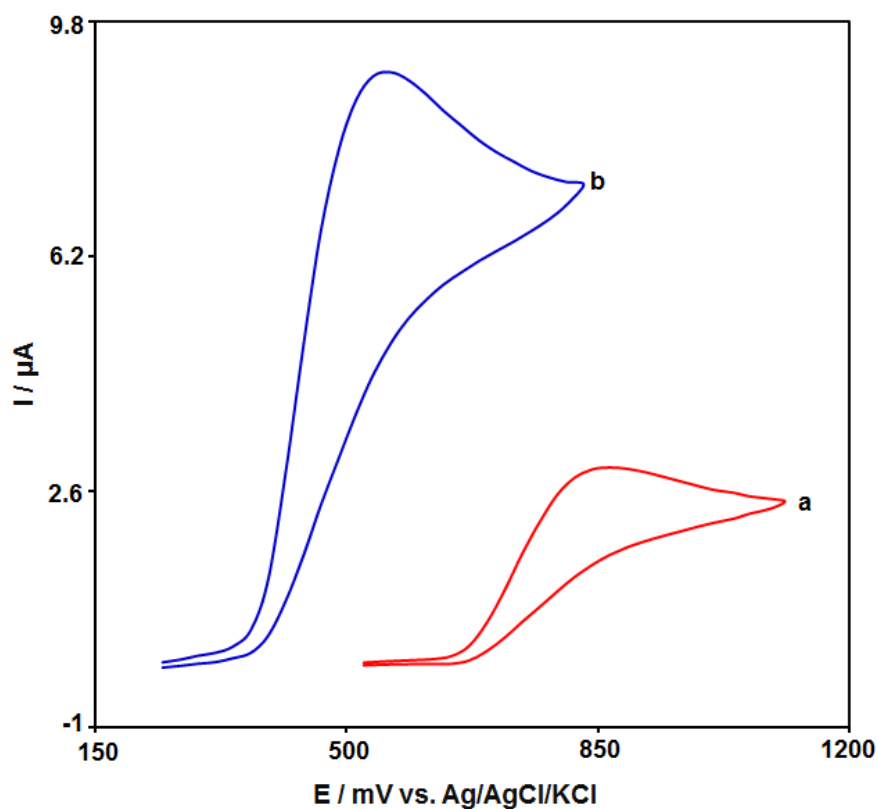
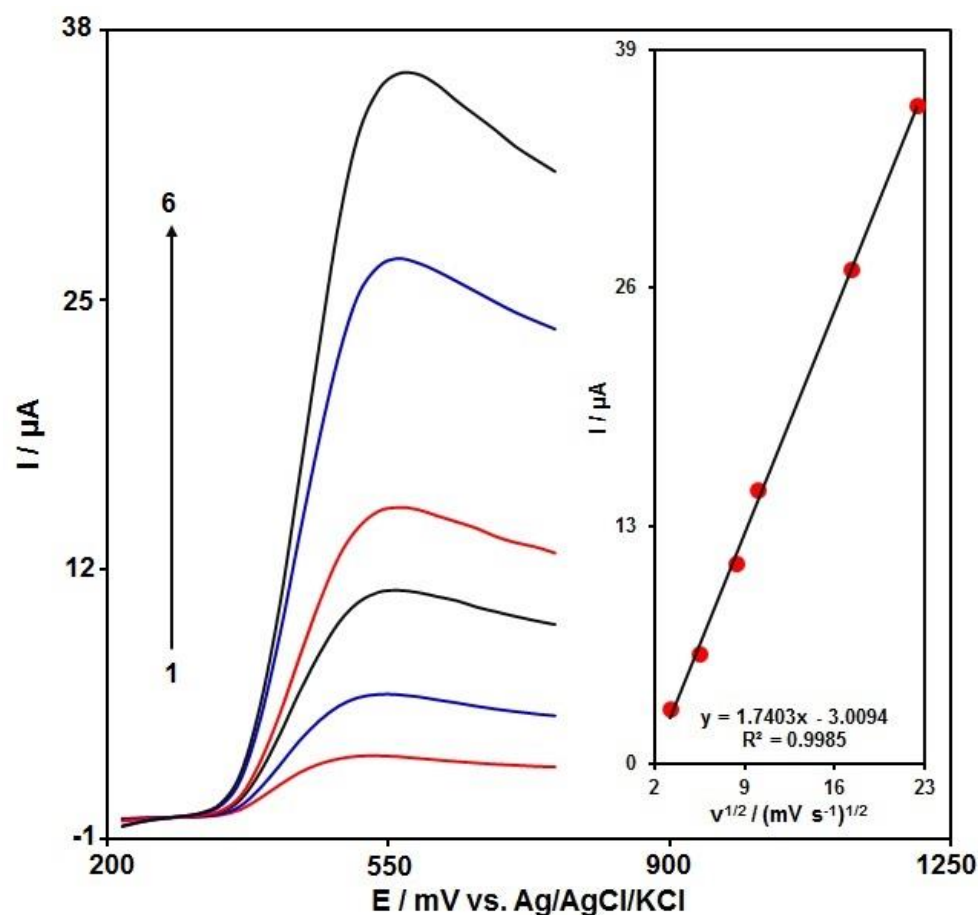


Figure 5. Cyclic voltammograms captured for N-rGO/GCE (a) and bare GCE (b) in PBS (0.1 M) at the optimized pH value of 7.0 in exposure to 100.0 μM of amaranth at 50 mV/s scan rate.

### 3.3. The Effects of the Scan Rate

We investigated the effect of the scan rate on the amaranth oxidation peak to analyze the electrode processes. We recorded the linear sweep voltammograms (LSVs) for 100.0  $\mu\text{M}$  of amaranth in PBS (0.1 M) at different scan rates. We found a linear dependence of the anodic peak currents on the square root of the scan rate (Figure 6). Such a finding led us to identify the diffusion-controlled process as the process responsible for amaranth oxidation on N-rGO/GCE.



**Figure 6.** LSVs captured for N-rGO/GCE in PBS (0.1 M) at the optimized pH value of 7.0 in exposure to 100.0  $\mu\text{M}$  of amaranth at various scan rates; (1): 10, (2): 30, (3): 70, (4): 100, (5): 300, and (6): 500  $\text{mV/s}$ , sequentially; inset: changes in anodic peak currents against  $v^{1/2}$ .

### 3.4. Chronoamperometric Measurements

Chronoamperometric analysis (Figure 7) is applied to calculate the diffusion coefficient of amaranth. As displayed in Figure 7 (A), the  $I$  vs.  $t^{-1/2}$  plots have been utilized for the optimal fits of different amaranth contents in PBS (0.1 M). Using various amaranth contents on N-rGO/GCE, we performed chronoamperometric measurements with the working electrode at the potential of 0.6 V. The slopes of the obtained straight lines versus amaranth contents were drawn to exploit the Cottrell equation below:

$$I = nFAD^{1/2}C_b\pi^{-1/2}t^{-1/2}$$

where  $D$  ( $\text{cm}^2/\text{s}$ ) is the diffusion coefficient and  $C_b$  ( $\text{mol}/\text{cm}^3$ ) indicates the bulk content. There was a linearity for the  $I$  plots against  $t^{-1/2}$  under diffusion control over various amaranth contents. We used the slope vs. amaranth content plot (Figure 7 (B)) to extract the mean  $D$  value for amaranth, obtaining  $2.5 \times 10^{-5} \text{ cm}^2/\text{s}$ .

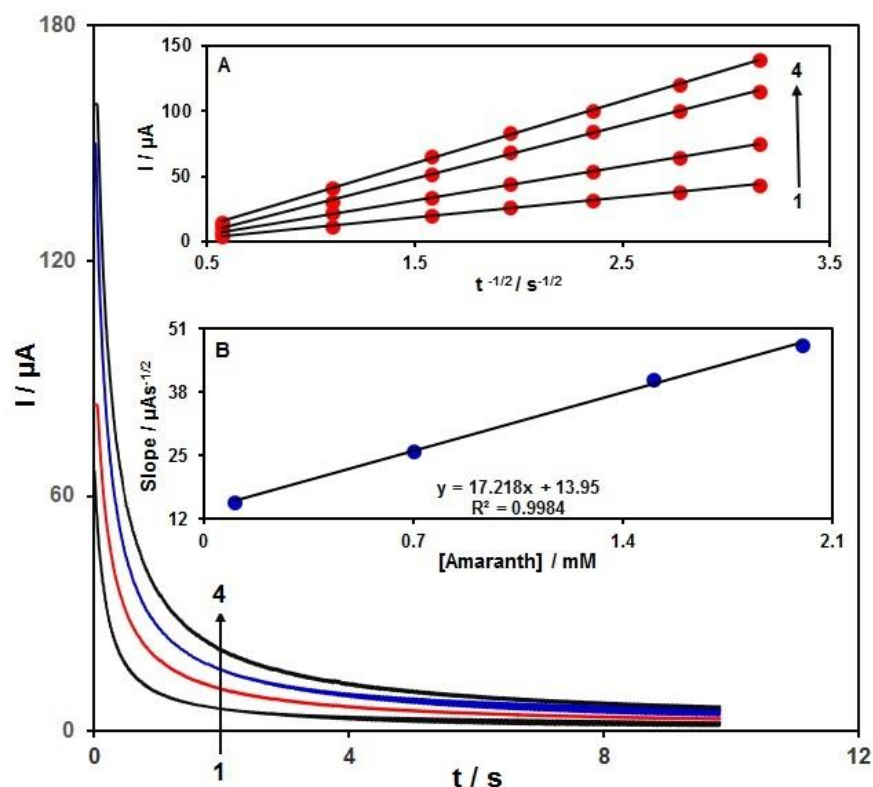


**Figure 7.** Chronoamperograms for N-rGO/GCE in PBS (0.1 M) at the optimized pH 7.0 for different amaranth contents; (1): 0.1, (2): 0.5, (3): 1.5, and (4): 2.0 mM of amaranth; insets: (A)  $I$  against  $t^{-1/2}$  plots from chronoamperograms 1 to 4. (B) Plot of straight line slope versus amaranth content.

### 3.5. Calibration Plot and LOD

Amaranth content was measured by the DPV technique. The DPVs captured for N-rGO/GCE at various amaranth contents in PBS (0.1 M) are shown in Figure 8. There was a stepwise enhancement in the amaranth oxidation current by gradually increasing amaranth contents, meaning the applicability of N-rGO/GCE for electrochemically sensing the amaranth. Figure 8 (inset) represents the alterations in the oxidation signal on N-rGO/GCE as a function of various amaranth contents (0.1–600.0  $\mu\text{M}$ ), having a low LOD of 0.03  $\mu\text{M}$ . In addition, Table 1 shows that the N-rGO/GCE can compete with other sensors for the determination of amaranth.

**Table 1.** Linear range and LOD obtained at the N-rGO/GCE for the determination of amaranth compared with other sensors.

Electrochemical Sensor	Method	Linear Range	LOD	Ref.
$\text{Fe}_3\text{O}_4$ @reduced graphene oxide/GCE	DPV	0.05–50 $\mu\text{M}$	50 nM	[2]
Ordered mesoporous carbon/GCE	DPV	$1.0 \times 10^{-7}$ – $3.0 \times 10^{-6}$ M	$3.2 \times 10^{-8}$ M	[3]
Single-walled carbon nanotube-titanium nitride nanocomposite/GCE	DPV	0.1–100 $\mu\text{M}$	40 nM	[67]
Multi-wall carbon nanotube thin film/GCE	DPV	40 nM–0.8 $\mu\text{M}$	35 nM	[68]
$\text{Co}_3\text{O}_4$ - $\text{CeO}_2$ /graphene nanocomposite modified electrode	DPV	2–96 $\mu\text{M}$	0.1591 $\mu\text{M}$	[69]
N-rGO/GCE	DPV	0.1–600.0 $\mu\text{M}$	0.03 $\mu\text{M}$	This Work

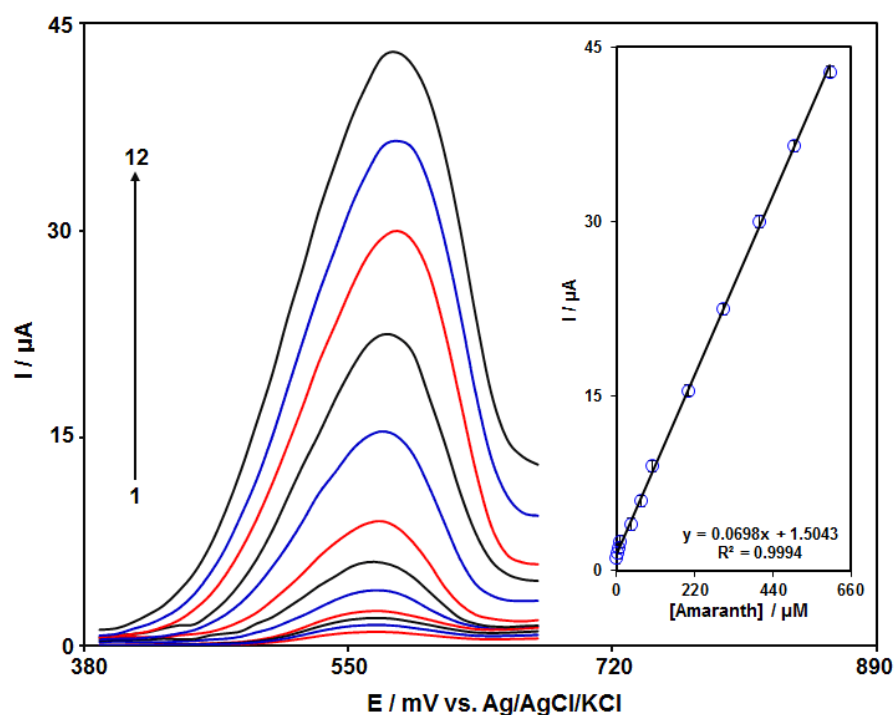


**Figure 8.** DPVs captured for N-rGO/GCE in PBS (0.1 M) at the optimized pH 7.0 in exposure to various amaranth contents; (1): 0.1, (2): 1.0, (3): 5.0, (4): 10.0, (5): 40.0, (6): 70.0, (7): 100.0, (8): 200.0, (9): 300.0, (10): 400.0, (11): 500.0, and (12): 600.0  $\mu\text{M}$  of amaranth; inset: peak current versus various amaranth contents (0.1–600.0  $\mu\text{M}$ ).

### 3.6. Analysing the Real Sample

The ability of N-rGO/GCE for sensor applications in the detection of amaranth was determined in real specimens of tap water, apple juice, and orange juice according to the standard addition method, as seen in Table 2. The recorded recovery rates ranged from 96.0% to 104.3%, thereby highlighting the appreciable applicability of N-rGO/GCE in sensing amaranth in real specimens.

**Table 2.** The application of N-rGO/GCE for the determination of amaranth in tap water, apple juice, and orange juice. ( $n = 5$ ).

Sample	Spiked ( $\mu\text{M}$ )	Found ( $\mu\text{M}$ )	Recovery (%)	R.S.D. (%)
Tap Water	0	-	-	-
	5.0	4.9	98.0	3.2
	6.0	6.2	103.3	1.7
	7.0	7.1	101.4	2.4
	8.0	7.8	97.5	2.6
Apple Juice	0	-	-	-
	4	4.1	102.5	1.7
	6	5.8	96.7	3.5
	8	8.1	101.2	2.6
	10	9.9	99.0	2.7
Orange Juice	0	-	-	-
	5	4.8	96.0	3.6
	7.0	7.3	104.3	2.8
	9.0	9.1	101.1	3.0
	11.0	10.9	99.1	1.9

#### 4. Conclusions

In this study, we developed a novel sensitive electrochemical sensor, based on N-rGO sheets, for the detection of amaranth. The proposed sensor exhibits remarkable electrocatalytic activity and excellent sensitivity toward amaranth detection with a linear response over a wide concentration range (0.1–600.0  $\mu\text{M}$ ) and a low detection limit (0.03  $\mu\text{M}$ ). Moreover, the applicability of N-rGO modified GCE was tested in real samples with good accuracy and satisfying recovery.

**Author Contributions:** Conceptualization, H.B. and A.D.B.; methodology, H.M., F.G.N. and H.B.; software, H.M.; validation, H.B. and A.D.B.; formal analysis, H.M., F.G.N. and A.D.B.; investigation, H.M., F.G.N. and H.B.; resources, H.B.; data curation, H.M., F.G.N. and H.B.; writing—original draft preparation, H.M. and H.B.; writing—review and editing, A.D.B.; visualization, H.M. and F.G.N.; supervision, H.B. and A.D.B.; project administration, H.B.; funding acquisition, H.B. and F.G.N. All authors have read and agreed to the published version of the manuscript.

**Funding:** This research was financially supported by the University of Salerno through grants ORSA218189 and ORSA200207. The APC was funded by A.D.B.

**Institutional Review Board Statement:** Not applicable.

**Informed Consent Statement:** Not applicable.

**Data Availability Statement:** The data presented in this study are available upon request from the corresponding authors.

**Conflicts of Interest:** The authors declare no conflict of interest.

#### References

1. Akbari, S. A new voltammetric sensor according to graphene quantum dots/ionic liquid modified carbon paste electrode for amaranth sensitive determination. *Int. J. Environ. Anal. Chem.* **2022**, *102*, 789–803. [[CrossRef](#)]
2. Han, Q.; Wang, X.; Yang, Z.; Zhu, W.; Zhou, X.; Jiang, H. Fe<sub>3</sub>O<sub>4</sub>@rGO doped molecularly imprinted polymer membrane based on magnetic field directed self-assembly for the determination of amaranth. *Talanta* **2014**, *123*, 101–108. [[CrossRef](#)] [[PubMed](#)]
3. Jian, J.U.; Li-Ping, G.U.O. Sensitive voltammetric sensor for amaranth based on ordered mesoporous carbon. *Chin. J. Anal. Chem.* **2013**, *41*, 681–686.
4. Li, L.; Zheng, H.; Guo, L.; Qu, L.; Yu, L. A sensitive and selective molecularly imprinted electrochemical sensor based on Pd-Cu bimetallic alloy functionalized graphene for detection of amaranth in soft drink. *Talanta* **2019**, *197*, 68–76. [[CrossRef](#)]
5. Jing, S.; Zheng, H.; Zhao, L.; Qu, L.; Yu, L. Electrochemical sensor based on poly (sodium 4-styrenesulfonate) functionalized graphene and Co<sub>3</sub>O<sub>4</sub> nanoparticle clusters for detection of amaranth in soft drinks. *Food Anal. Methods* **2017**, *10*, 3149–3157. [[CrossRef](#)]
6. Biswas, S.; Harwansh, R.K.; Kar, A.; Mukherjee, P.K. Validated high-performance thin-layer chromatographic method for the simultaneous determination of quercetin, rutin, and gallic acid in *Amaranthus tricolor* L. *JPC-J. Planar Chroma* **2019**, *32*, 121–126. [[CrossRef](#)]
7. Alves, S.P.; Brum, D.M.; de Andrade, É.C.B.; Netto, A.D.P. Determination of synthetic dyes in selected foodstuffs by high performance liquid chromatography with UV-DAD detection. *Food Chem.* **2008**, *107*, 489–496. [[CrossRef](#)]
8. Kim, H.J.; Lee, M.J.; Park, H.J.; Kim, H.J.; Cho, S.K.; Jeong, M.H. Simultaneous determination of synthetic food additives in kimchi by liquid chromatography-electrospray tandem mass spectrometry. *Food Sci. Biotechnol.* **2018**, *27*, 877–882. [[CrossRef](#)]
9. El-Zomrawy, A.A. Selective and sensitive spectrophotometric method to determine trace amounts of copper metal ions using Amaranth food dye. *Spectrochim. Acta A Mol. Biomol. Spectrosc.* **2018**, *203*, 450–454. [[CrossRef](#)]
10. Sha, O.; Zhu, X. Simultaneous ionic liquid aqueous two-phase extraction and spectrophotometric determination of amaranth and brilliant blue in food samples. *J. Anal. Chem.* **2015**, *70*, 558–565. [[CrossRef](#)]
11. Yi, J.; Zeng, L.; Wu, Q.; Yang, L.; Xie, T. Sensitive simultaneous determination of synthetic food colorants in preserved fruit samples by capillary electrophoresis with contactless conductivity detection. *Food Anal. Methods* **2018**, *11*, 1608–1618. [[CrossRef](#)]
12. Pogacean, F.; Rosu, M.C.; Coros, M.; Magerusan, L.; Moldovan, M.; Sarosi, C.; Porav, A.S.; Stefan-van Staden, R.I.; Pruneanu, S. Graphene/TiO<sub>2</sub>-Ag based composites used as sensitive electrode materials for amaranth electrochemical detection and degradation. *J. Electrochem. Soc.* **2018**, *165*, B3054. [[CrossRef](#)]
13. Zhang, Q.; Cheng, W.; Wu, D.; Yang, Y.; Feng, X.; Gao, C.; Meng, L.; Shen, X.; Zhang, Y.; Tang, X. An electrochemical method for determination of amaranth in drinks using functionalized graphene oxide/chitosan/ionic liquid nanocomposite supported nanoporous gold. *Food Chem.* **2022**, *367*, 130727. [[CrossRef](#)]
14. Shetti, N.P.; Bukkitgar, S.D.; Reddy, K.R.; Reddy, C.V.; Aminabhavi, T.M. ZnO-based nanostructured electrodes for electrochemical sensors and biosensors in biomedical applications. *Biosens. Bioelectron.* **2019**, *141*, 111417. [[CrossRef](#)]

15. Payehghadr, M.; Taherkhani, Y.; Maleki, A.; Nourifard, F. Selective and sensitive voltammetric sensor for methocarbamol determination by molecularly imprinted polymer modified carbon paste electrode. *Eurasian Chem. Commun.* **2020**, *2*, 982–990.
16. Eren, T.; Atar, N.; Yola, M.L.; Karimi-Maleh, H. A sensitive molecularly imprinted polymer based quartz crystal microbalance nanosensor for selective determination of lovastatin in red yeast rice. *Food Chem.* **2015**, *185*, 430–436. [[CrossRef](#)]
17. Shen, C.; Liu, S.; Li, X.; Yang, M. Electrochemical detection of circulating tumor cells based on DNA generated electrochemical current and rolling circle amplification. *Anal. Chem.* **2019**, *91*, 11614–11619. [[CrossRef](#)]
18. Mohanraj, J.; Durgalakshmi, D.; Rakkesh, R.A.; Balakumar, S.; Rajendran, S.; Karimi-Maleh, H. Facile synthesis of paper based graphene electrodes for point of care devices: A double stranded DNA (dsDNA) biosensor. *J. Colloid Interface Sci.* **2020**, *566*, 463–472. [[CrossRef](#)]
19. Tajik, S.; Dourandish, Z.; Garkani-Nejad, F.; Aghaei Afshar, A.; Beitollahi, H. Voltammetric determination of isoniazid in the presence of acetaminophen utilizing MoS<sub>2</sub>-nanosheet-modified screen-printed electrode. *Micromachines* **2022**, *13*, 369. [[CrossRef](#)]
20. Deshmukh, M.A.; Celiesiute, R.; Ramanaviciene, A.; Shirsat, M.D.; Ramanavicius, A. EDTA\_PANI/SWCNTs nanocomposite modified electrode for electrochemical determination of copper (II), lead (II) and mercury (II) ions. *Electrochim. Acta* **2018**, *259*, 930–938. [[CrossRef](#)]
21. Raouf, J.B.; Ojani, R.; Beitollahi, H.; Hosseinzadeh, R. Electrocatalytic oxidation and highly selective voltammetric determination of L-cysteine at the surface of a 1-[4-(ferrocenyl ethynyl) phenyl]-1-ethanone modified carbon paste electrode. *Anal. Sci.* **2006**, *22*, 1213–1220. [[CrossRef](#)]
22. Tajik, S.; Askari, M.B.; Ahmadi, S.A.; Garkani-Nejad, F.; Dourandish, Z.; Razavi, R.; Beitollahi, H.; Di Bartolomeo, A. Electrochemical sensor based on ZnFe<sub>2</sub>O<sub>4</sub>/RGO nanocomposite for ultrasensitive detection of hydrazine in real samples. *Nanomaterials* **2022**, *12*, 491. [[CrossRef](#)]
23. Yang, L.; Xu, C.; Ye, W.; Liu, W. An electrochemical sensor for H<sub>2</sub>O<sub>2</sub> based on a new Co-metal-organic framework modified electrode. *Sens. Actuators B Chem.* **2015**, *215*, 489–496. [[CrossRef](#)]
24. Elobeid, W.H.; Elbashir, A.A. Development of chemically modified pencil graphite electrode based on benzo-18-crown-6 and multi-walled CNTs for determination of lead in water samples. *Prog. Chem. Biochem. Res.* **2019**, *2*, 24–33.
25. Shahsavari, M.; Tajik, S.; Sheikhshoae, I.; Garkani-Nejad, F.; Beitollahi, H. Synthesis of Fe<sub>3</sub>O<sub>4</sub>@copper (II) imidazolate nanoparticles: Catalytic activity of modified graphite screen printed electrode for the determination of levodopa in presence of melatonin. *Microchem. J.* **2021**, *170*, 106637. [[CrossRef](#)]
26. Montazarolmahdi, M.; Masrounia, M.; Nezhadali, A. A new electrochemical approach for the determination of phenylhydrazine in water and wastewater samples using amplified carbon paste electrode. *Chem. Methodol.* **2020**, *4*, 732–742.
27. Karimi-Maleh, H.; Khataee, A.; Karimi, F.; Baghayeri, M.; Fu, L.; Rouhi, J.; Karaman, C.; Karaman, O.; Boukherroub, R. A green and sensitive guanine-based DNA biosensor for idarubicin anticancer monitoring in biological samples: A simple and fast strategy for control of health quality in chemotherapy procedure confirmed by docking investigation. *Chemosphere* **2022**, *291*, 132928. [[CrossRef](#)]
28. Karimi-Maleh, H.; Karimi, F.; Orooji, Y.; Mansouri, G.; Razmjou, A.; Aygun, A.; Sen, F. A new nickel-based co-crystal complex electrocatalyst amplified by NiO dope Pt nanostructure hybrid; a highly sensitive approach for determination of cysteamine in the presence of serotonin. *Sci. Rep.* **2020**, *10*, 11699. [[CrossRef](#)]
29. Abrishamkar, M.; Ehsani Tilami, S.; Hosseini Kaldozakh, S. Electrocatalytic oxidation of cefixime at the surface of modified carbon paste electrode with synthesized nano zeolite. *Adv. J. Chem. A* **2020**, *3*, 767–776.
30. Tajik, S.; Shahsavari, M.; Sheikhshoae, I.; Garkani Nejad, F.; Beitollahi, H. Voltammetric detection of sumatriptan in the presence of naproxen using Fe<sub>3</sub>O<sub>4</sub>@ZIF-8 nanoparticles modified screen printed graphite electrode. *Sci. Rep.* **2021**, *11*, 24068. [[CrossRef](#)]
31. Miraki, M.; Karimi-Maleh, H.; Taher, M.A.; Cheraghi, S.; Karimi, F.; Agarwal, S.; Gupta, V.K. Voltammetric amplified platform based on ionic liquid/NiO nanocomposite for determination of benserazide and levodopa. *J. Mol. Liq.* **2019**, *278*, 672–676. [[CrossRef](#)]
32. Ahmadi, R. Investigating the performance of nano structure C60 as nano-carriers of anticancer cytarabine, a DFT study. *Asian J. Green Chem.* **2020**, *4*, 355–366.
33. Saeidi, S.; Javadian, F.; Sepehri, Z.; Shahi, Z.; Mousavi, F.; Anbari, M. Antibacterial effects of silver nanoparticles against resistant strains of E. coli bacteria. *Int. J. Adv. Biol. Biomed. Res.* **2016**, *4*, 96–99.
34. Karimi-Maleh, H.; Darabi, R.; Shabani-Nooshabadi, M.; Baghayeri, M.; Karimi, F.; Rouhi, J.; Karaman, C. Determination of D&C Red 33 and Patent Blue V Azo dyes using an impressive electrochemical sensor based on carbon paste electrode modified with ZIF-8/g-C<sub>3</sub>N<sub>4</sub>/Co and ionic liquid in mouthwash and toothpaste as real samples. *Food Chem. Toxicol.* **2022**, *162*, 112907.
35. Shaikh, U.U.; Tamboli, Q.; Pathange, S.M.; Dahan, Z.A.; Pudukulathan, Z. An efficient method for chemoselective acetylation of activated alcohols using nano ZnFe<sub>2</sub>O<sub>4</sub> as catalyst. *Chem. Methodol.* **2018**, *2*, 73–82.
36. Fazal-ur-Rehman, M.; Qayyum, I. Biomedical scope of gold nanoparticles in medical sciences; an advancement in cancer therapy. *J. Med. Chem. Sci.* **2020**, *3*, 399–407.
37. Karimi-Maleh, H.; Karaman, C.; Karaman, O.; Karimi, F.; Vasseghian, Y.; Fu, L.; Mirabi, A. Nanochemistry approach for the fabrication of Fe and N co-decorated biomass-derived activated carbon frameworks: A promising oxygen reduction reaction electrocatalyst in neutral media. *J. Nanostruct. Chem.* **2022**. [[CrossRef](#)]
38. Sheikhshoae, I.; Rezaadeh, A.; Ramezanpour, S. Removal of Pb (II) from aqueous solution by gel combustion of a new nano sized Co<sub>3</sub>O<sub>4</sub>/ZnO composite. *Asian J. Nanosci. Mater.* **2018**, *1*, 271–281.

39. Abegunde, S.M.; Idowu, K.S.; Sulaimon, A.O. Plant-mediated iron nanoparticles and their applications as adsorbents for water treatment—a review. *J. Chem. Rev.* **2020**, *2*, 103–113. [[CrossRef](#)]
40. Karimi-Maleh, H.; Sheikhshoaie, M.; Sheikhshoaie, I.; Ranjbar, M.; Alizadeh, J.; Maxakato, N.W.; Abbaspourrad, A. A novel electrochemical epinine sensor using amplified CuO nanoparticles and an-hexyl-3-methylimidazolium hexafluorophosphate electrode. *New J. Chem.* **2019**, *43*, 2362–2367. [[CrossRef](#)]
41. Alavi-Tabari, S.A.; Khalilzadeh, M.A.; Karimi-Maleh, H. Simultaneous determination of doxorubicin and dasatinib as two breast anticancer drugs uses an amplified sensor with ionic liquid and ZnO nanoparticle. *J. Electroanal. Chem.* **2018**, *811*, 84–88. [[CrossRef](#)]
42. Wang, Y.; Qiao, M.; Mamat, X.; Hu, X.; Hu, G. Hierarchically ordered porous nitrogen doped carbon modified a glassy carbon electrode for voltammetry detection of quercetin. *Mater. Res. Bull.* **2021**, *136*, 111131. [[CrossRef](#)]
43. Tajik, S.; Beitollahi, H.; Shahsavari, S.; Garkani-Nejad, F. Simultaneous and selective electrochemical sensing of methotrexate and folic acid in biological fluids and pharmaceutical samples using Fe<sub>3</sub>O<sub>4</sub>/ppy/Pd nanocomposite modified screen printed graphite electrode. *Chemosphere* **2022**, *291*, 132736. [[CrossRef](#)]
44. Askari, M.B.; Salarizadeh, P.; Di Bartolomeo, A.; Şen, F. Enhanced electrochemical performance of MnNi<sub>2</sub>O<sub>4</sub>/rGO nanocomposite as pseudocapacitor electrode material and methanol electro-oxidation catalyst. *Nanotechnology* **2021**, *32*, 325707. [[CrossRef](#)]
45. Sengar, M.; Saxena, S.; Satsangee, S.; Jain, R. Silver nanoparticles decorated functionalized multiwalled carbon nanotubes modified screen printed sensor for the voltammetric determination of butorphanol. *J. Appl. Organomet. Chem.* **2021**, *1*, 95–108.
46. Karimi-Maleh, H.; Shojaei, A.F.; Tabatabaiean, K.; Karimi, F.; Shakeri, S.; Moradi, R. Simultaneous determination of 6-mercaptopyruvate, 6-thioguanine and dasatinib as three important anticancer drugs using nanostructure voltammetric sensor employing Pt/MWCNTs and 1-butyl-3-methylimidazolium hexafluoro phosphate. *Biosens. Bioelectron.* **2016**, *86*, 879–884. [[CrossRef](#)]
47. Mahmoudi-Moghaddam, H.; Beitollahi, H.; Tajik, S.; Sheikhshoaie, I.; Biparva, P. Fabrication of novel TiO<sub>2</sub> nanoparticles/Mn (III) salen doped carbon paste electrode: Application as electrochemical sensor for the determination of hydrazine in the presence of phenol. *Environ. Monit. Assess.* **2015**, *187*, 407. [[CrossRef](#)]
48. Prasad, P.; Sreedhar, N.Y. Effective SWCNTs/Nafion electrochemical sensor for detection of dicapthon pesticide in water and agricultural food samples. *Chem. Methodol.* **2018**, *2*, 277–290.
49. Urban, F.; Lupina, G.; Grillo, A.; Martucciello, N.; Di Bartolomeo, A. Contact resistance and mobility in back-gate graphene transistors. *Nano Express* **2020**, *1*, 010001. [[CrossRef](#)]
50. Bhardiya, S.R.; Asati, A.; Sheshma, H.; Rai, A.; Rai, V.K.; Singh, M. A novel bioconjugated reduced graphene oxide-based nanocomposite for sensitive electrochemical detection of cadmium in water. *Sens. Actuators B Chem.* **2021**, *328*, 129019. [[CrossRef](#)]
51. Yang, S.; Liu, P.; Wang, Y.; Guo, Z.; Tan, R.; Qu, L. Electrochemical sensor using poly-(L-cysteine) functionalized CuO nanoneedles/N-doped reduced graphene oxide for detection of lead ions. *RSC Adv.* **2020**, *10*, 18526–18532. [[CrossRef](#)]
52. Beitollahi, H.; Garkani-Nejad, F. Voltammetric determination of vitamin B6 (pyridoxine) at a graphite screen-printed electrode modified with graphene oxide/Fe<sub>3</sub>O<sub>4</sub>@SiO<sub>2</sub> nanocomposite. *Russ. Chem. Bull.* **2018**, *67*, 238–242. [[CrossRef](#)]
53. Barsan, M.M.; Prathish, K.P.; Sun, X.; Brett, C.M. Nitrogen doped graphene and its derivatives as sensors and efficient direct electron transfer platform for enzyme biosensors. *Sens. Actuators B Chem.* **2014**, *203*, 579–587. [[CrossRef](#)]
54. Keteklahijani, Y.Z.; Sharif, F.; Roberts, E.P.; Sundararaj, U. Enhanced sensitivity of dopamine biosensors: An electrochemical approach based on nanocomposite electrodes comprising polyaniline, nitrogen-doped graphene, and DNA-functionalized carbon nanotubes. *J. Electrochem. Soc.* **2019**, *166*, B1415. [[CrossRef](#)]
55. Jia, H.; Yang, T.; Zuo, Y.; Wang, W.; Xu, J.; Lu, L.; Li, P. Immunosensor for  $\alpha$ -fetoprotein based on a glassy carbon electrode modified with electrochemically deposited N-doped graphene, gold nanoparticles and chitosan. *Microchim. Acta* **2017**, *184*, 3747–3753. [[CrossRef](#)]
56. Zou, C.E.; Bin, D.; Yang, B.; Zhang, K.; Du, Y. Rutin detection using highly electrochemical sensing amplified by an Au–Ag nanoring decorated N-doped graphene nanosheet. *RSC Adv.* **2016**, *6*, 107851–107858. [[CrossRef](#)]
57. Yang, W.; Zhou, M.; Liang, L. Highly efficient in-situ metal-free electrochemical advanced oxidation process using graphite felt modified with N-doped graphene. *Chem. Eng. J.* **2018**, *338*, 700–708. [[CrossRef](#)]
58. Di Bartolomeo, A.; Giubileo, F.; Romeo, F.; Sabatino, P.; Carapella, G.; Iemmo, L.; Schroeder, T.; Lupina, G. Graphene field effect transistors with niobium contacts and asymmetric transfer characteristics. *Nanotechnology* **2015**, *26*, 475202. [[CrossRef](#)]
59. Salahandish, R.; Ghaffarinejad, A.; Omidinia, E.; Zargartalebi, H.; Majidzadeh, K.; Naghib, S.M.; Sanati-Nezhad, A. Label-free ultrasensitive detection of breast cancer miRNA-21 biomarker employing electrochemical nano-genosensor based on sandwiched AgNPs in PANI and N-doped graphene. *Biosens. Bioelectron.* **2018**, *120*, 129–136. [[CrossRef](#)]
60. Gong, Y.; Li, D.; Fu, Q.; Pan, C. Influence of graphene microstructures on electrochemical performance for supercapacitors. *Prog. Nat. Sci. Mat. Int.* **2015**, *25*, 379–385. [[CrossRef](#)]
61. Zhao, K.; Gu, W.; Zhao, L.; Zhang, C.; Peng, W.; Xian, Y. MoS<sub>2</sub>/Nitrogen-doped graphene as efficient electrocatalyst for oxygen reduction reaction. *Electrochim. Acta* **2015**, *169*, 142–149. [[CrossRef](#)]
62. Fakude, C.T.; Arotiba, O.A.; Moutloali, R.; Mabuba, N. Nitrogen-doped graphene electrochemical sensor for selenium (IV) in water. *Int. J. Electrochem. Sci.* **2019**, *14*, 9391–9403. [[CrossRef](#)]

63. Liu, Y.; Ma, J.; Wu, T.; Wang, X.; Huang, G.; Liu, Y.; Qiu, H.; Li, Y.; Wang, W.; Gao, J. Cost-effective reduced graphene oxide-coated polyurethane sponge as a highly efficient and reusable oil-absorbent. *ACS Appl. Mater. Interfaces* **2013**, *5*, 10018–10026. [[CrossRef](#)] [[PubMed](#)]
64. Rahmani, Z.; Rashidi, A.M.; Samadi, M.T.; Rahmani, A.R. N-doped reduced graphene oxide aerogel for the selective adsorption of oil pollutants from water: Isotherm and kinetic study. *J. Ind. Eng. Chem.* **2018**, *61*, 416–426. [[CrossRef](#)]
65. Fan, H.; Li, Y.; Wu, D.; Ma, H.; Mao, K.; Fan, D.; Wei, Q. Electrochemical bisphenol A sensor based on N-doped graphene sheets. *Anal. Chim. Acta* **2012**, *711*, 24–28. [[CrossRef](#)]
66. Rahsepar, M.; Foroughi, F.; Kim, H. A new enzyme-free biosensor based on nitrogen-doped graphene with high sensing performance for electrochemical detection of glucose at biological pH value. *Sens. Actuators B Chem.* **2019**, *282*, 322–330. [[CrossRef](#)]
67. He, J.L.; Kou, W.; Li, C.; Cai, J.J.; Kong, F.Y.; Wang, W. Electrochemical sensor based on single-walled carbon nanotube-TiN nanocomposites for detecting Amaranth. *Int. J. Electrochem. Sci.* **2015**, *10*, 10074–10082.
68. Wang, P.; Hu, X.; Cheng, Q.; Zhao, X.; Fu, X.; Wu, K. Electrochemical detection of amaranth in food based on the enhancement effect of carbon nanotube film. *J. Agric. Food Chem.* **2010**, *58*, 12112–12116. [[CrossRef](#)]
69. Wang, H.; Zhu, S.; Liu, C.; Gu, L.; Chang, J.; Xie, A.; Luo, S. Co<sub>3</sub>O<sub>4</sub>-CeO<sub>2</sub>/Graphene Composite as a Novel Sensor for Amaranth Detection. *J. Electrochem. Soc.* **2021**, *168*, 027513. [[CrossRef](#)]